Transport and Communications Science Journal, Vol. 77, Issue 09 (11/2026), 1211-1225

Transport and Communications Science Journal

MULTI-RESPONSE OPTIMIZATION IN COLD METAL TRANSFER WIRE ARC ADDITIVE MANUFACTURING OF INCONEL 718 THIN WALLS

Van Thao Le[1,*], Chi Tinh Phung[2], Manh Tung Do[3], Dinh Si Mai[1], Van Son Nguyen[1], Ba Tinh Do[4], Manh Cuong Bui[3], Tat Khoa Doan[3]

[1] Advanced Technology Center, Le Quy Don Technical University, Hanoi, Vietnam

[2] Weapon Institute, Hanoi, Vietnam

[3] Faculty of Mechanical Engineering, Le Quy Don Technical University, Hanoi, Vietnam

[4] Institute of Technology, Hanoi, Vietnam

ARTICLE INFO

TYPE: Research Article
Received: 25/03/2026
Revised: 03/11/2026
Accepted: 10/11/2026
Published online: 15/11/2026
https://doi.org/10.47869/tcsj.77.9.7
[*] *Corresponding author*
Email: vtle@lqdtu.edu.vn

Abstract. Wire arc additive manufacturing (WAAM) of Inconel 718 thin walls requires careful parameter selection to balance geometric accuracy and surface quality. In this study, the effects of wire feed speed (*wfs*) and travel speed (*v*) on the effective width (*EW*), total height (*TH*), and surface roughness (S_a) of 20-layer walls fabricated by cold metal transfer (CMT)-WAAM process were first analyzed through a full factorial experiment design. To resolve the trade-off between productivity and surface integrity, a multi-criteria decision-making framework integrating Entropy weight method (EWM) with COPRAS and WASPAS methods was applied. The analysis of variance (ANOVA) results reveal that *wfs* primarily governs *EW*, while *v* dominates *TH* and S_a. Both COPRAS and WASPAS optimization techniques consistently identify *wfs* = 6 m/min and *v* = 40 cm/min as the optimal condition, achieving high deposition height with acceptable surface roughness. The proposed framework offers a robust strategy for optimization in CMT-WAAM of Inconel 718 superalloys.

Keywords: CMT-WAAM, Inconel 718, thin wall, optimization, COPRAS, WASPAS.

@ 2026 University of Transport and Communications

1. INTRODUCTION

Additive manufacturing (AM) has emerged as a pivotal technology in modern engineering, enabling the fabrication of complex metallic components through layer-by-layer material deposition. Among metal AM technologies, wire arc additive manufacturing (WAAM) has attracted considerable attention because of its high deposition rate, high material utilization, and relatively low equipment cost, making it particularly suitable for medium- to large-scale components [1,2]. Nevertheless, achieving stable deposition and consistent geometric accuracy remains challenging, particularly in multilayer structures where the thermal history evolves continuously with the number of deposited layers [3]. Consequently, appropriate process-parameter selection is essential for controlling deposition geometry, surface quality, and overall process stability.

Among the process parameters, wire feed speed (*wfs*) and travel speed (*v*) are two primary factors governing material deposition rate, bead geometry, and heat input [4,5]. In general, *wfs* primarily determines the amount of material supplied to the molten pool, whereas *v* influences the amount of deposited material per unit length and the thermal conditions during deposition [6-8]. Their coupled effects therefore directly affect the width and height of deposited structures as well as surface morphology. Inadequate coordination between these parameters can result in irregular layer geometry and poor surface finish, and these effects may become more pronounced in multilayer structures because of cumulative heat accumulation and changes in molten-pool behavior [9]. Cold Metal Transfer (CMT) technology has been increasingly adopted in WAAM to improve deposition stability through controlled droplet transfer and relatively low heat input, thereby reducing spatter and improving bead uniformity [10]. Recently, data-driven modeling and multi-objective optimization methods have increasingly been employed to establish relationships between process parameters and deposition responses, including bead geometry and surface roughness [11-13].

Nickel-based superalloys, particularly Inconel 718, are widely used in aerospace and energy applications owing to their excellent high-temperature strength, corrosion resistance, and mechanical stability [10]. However, their poor machinability and high work-hardening tendency make conventional manufacturing challenging, motivating the use of additive manufacturing. In WAAM, inadequate thermal management of Inconel 718 can induce elemental segregation, porosity, and coarse-grained microstructures, adversely affecting component performance [14,15]. Previous studies have highlighted the significant effects of heat input, deposition strategy, and thermal history on the microstructure and mechanical properties of WAAM-fabricated Inconel 718 [10]. Nevertheless, the geometric stability of multilayer Inconel 718 structures produced by CMT-WAAM under coupled process-parameter variations remains insufficiently understood.

To address this gap, the present study investigates 20-layer Inconel 718 thin walls fabricated by CMT-WAAM using a full factorial experimental design. The coupled effects of wire feed speed (*wfs*) and travel speed (*v*) are systematically evaluated in terms of effective width (*EW*), total height (*TH*), and surface roughness (S_a), thereby providing a combined assessment of deposition geometry and surface quality. Because no predefined design dimensions were imposed for the deposited walls, *EW* and *TH* are used to characterize the resulting deposition capability rather than dimensional deviation from a nominal geometry. Subsequently, an integrated multi-criteria decision-making (MCDM) framework combining

the entropy weight method (EWM) with COPRAS and WASPAS is employed to rank the investigated process-parameter combinations. In the optimization, *EW* and *TH* are treated as larger-is-better responses, whereas Sa is treated as a smaller-is-better response, with the objective of achieving favorable wall build-up and surface quality simultaneously.

The main novelties of this study can be summarized in three aspects. First, it experimentally establishes the coupled effects of wfs and v on the deposition behavior of 20-layer Inconel 718 thin walls produced by CMT-WAAM, providing insight into parameter effects beyond single-bead or short-layer deposition. Second, *EW*, *TH*, and S_a are simultaneously incorporated as competing responses to evaluate the trade-off between wall geometry and surface quality during multilayer deposition. Third, an EWM-based COPRAS/WASPAS optimization framework is applied to identify and cross-evaluate the most desirable process-parameter combination, providing a systematic basis for multi-response parameter selection. The resulting framework is intended to provide practical guidance for improving dimensional consistency and surface quality in CMT-WAAM fabrication of Inconel 718 thin-wall structures.

2. METHODOLOGY

2.1. Experiment

In this research, a 1.2-mm-diameter Inconel 718 solid wire (KW-M718, Kiswel) was used as the filler material for the 20-layer wall deposition. The substrate used in the wall deposition is a low-carbon structural steel (EN 10025-2) with dimensions of 200 × 100 × 6 mm. The chemical compositions of both the substrate and filler material are listed in Table 1. Prior to deposition, the substrate surfaces were sandblasted and cleaned to remove oxides and contaminants, ensuring stable arc conditions and proper metallurgical bonding.

Table 1. Chemical composition of S235JR steel and Inconel 718 welding wire (by weight %).

Materials	C	Mn	Si	Cr	Mo	Nb+Ta	Ti	Al	Co	Ni	Fe
Inconel 718	≤ 0.08	≤ 0.35	≤ 0.35	17.0 - 21.0	2.8 - 3.3	4.75 - 5.50	0.65 - 1.15	0.20 - 0.80	≤ 1.0	50.0 - 55.0	Bal.
S235JR	≤ 0.17	≤ 1.4	≤ 0.5	≤ 0.3	≤ 0.08	≤ 0.05	≤ 0.03	≤ 0.02	-	≤ 0.3	Bal.

The CMT-WAAM system integrated a six-axis robot (FANUC Arc Mate 100iD) with a CMT power source (Fronius TPS 400i), as shown in Figure 1. The process operated in standard Cold Metal Transfer (CMT) mode, with a contact-tip-to-work distance of 15 mm and a torch angle of 90°. Deposition was performed under ambient conditions, utilizing synchronized wire retraction to achieve low-heat, spatter-free deposition, which is essential for minimizing thermal distortion in multilayer structures. Shielding was provided using high-purity argon gas at a constant flow rate of 15 L/min.

For CMT power sources, welding current and voltage are synergically linked to wire feed speed (*wfs*); thus, *wfs* and travel speed (*v*) were selected as primary decision variables in the experiments. The three levels of each parameter were selected based on the recommendation of the wire manufacturer and several trials (Table 2). A full factorial design was employed, resulting in nine experimental runs (Table 3).

For each run, a 20-layer thin-wall structure was fabricated using a zigzag deposition strategy with alternating travel direction to maintain geometric balance. This number of layers

was selected to represent a typical multi-layer WAAM structure where thermal accumulation effects become significant. A constant interlayer dwell time of 60 s was applied to control heat accumulation under ambient conditions. The wall geometry was characterized by effective width (*EW*), total height (*TH*), and surface roughness (S_a). *TH* reflects vertical buildup, *EW* represents the effective deposition width after excluding edge irregularities, and *Sa* characterizes surface roughness.



Figure 1. The CMT-WAAM system, including a 6-axis Fanuc robot arm, robot control cabinet, and a CMT power source (TPS400i).

Table 2. The levels of the input parameters.

Parameters	**Levels**		
wfs (m/min)	4	5	6
v (cm/min)	40	50	60

After deposition, the geometrical and surface characteristics were evaluated in terms of effective width (*EW*), total height (*TH*), and surface roughness (S_a). The total width (*TW*) and surface profile parameter (S_z) were initially measured to calculate the effective width (*EW*), which represents the functional deposition width by excluding edge irregularities. The surface morphology of the walls was captured by an ATOS optical 3D scanning system (Figure 2a). Data from a central 60 × 20 mm region of interest were processed in OmniSurf 3D software to determine S_a and S_z parameters (Figure 2c-2d-2e). For each deposited wall, *EW* and *TH* were measured at five locations distributed along the deposition direction to account for spatial variations in wall geometry, and the measurement of S_z and S_a was repeated three times for each wall side. The arithmetic mean of these measurements was used as the representative *EW*, *TH*, S_z, and S_a for each experimental condition.

The effective width (*EW*) represents the functional deposition width, calculated by subtracting bilateral surface irregularities from the total width [16,17]:

$$EW = TW - S_{z(\text{left})} - S_{z(\text{right})} \quad (1)$$

where *TW* is the total width, $S_{z(left)}$ and $S_{z(right)}$ are the maximum heights of surface irregularities on the left and right sides, respectively, obtained from 3D surface topography.

This definition eliminates edge irregularities and provides a more representative measure of the effective deposition width [16,17]. All the collected data for the analysis and the multi-response optimization was summarized in Table 3. Each experimental condition was performed once due to material and time constraints.

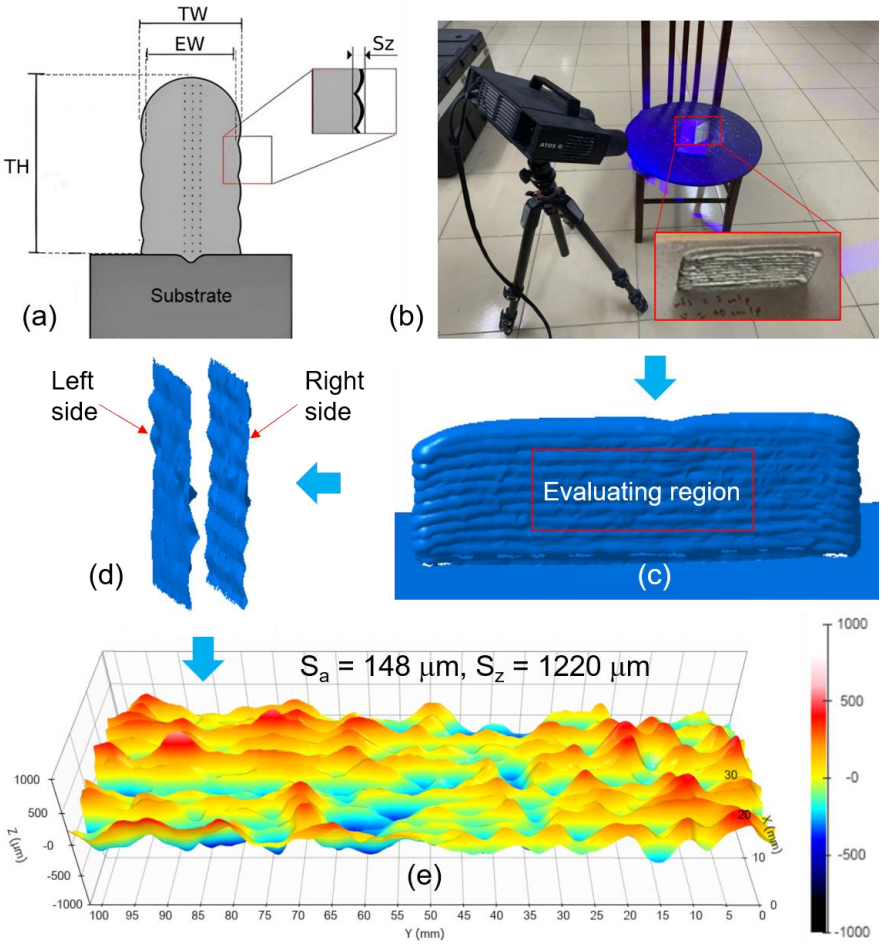


Figure 2. Data acquisition procedure: (a) description of output parameters (*TH*, *TW*, EW and S_z), (b) 3D scanning setup for surface geometry acquisition, (c) Stable region, (d) extracting left-side and right-side surfaces, and (e) evaluating 3D surface morphology with Omnisurf3D software.

Table 3. Experimental data for 20-layer Inconel 718 CMT-WAAM deposition.

Run No.	*wfs* (m/min)	*v* (cm/min)	*TW* (mm)	$S_{z(left)}$ (mm)	$S_{z(right)}$ (mm)	*EW* (mm)	*TH* (mm)	S_a (µm)
1	4	40	8.09	1.22	1.16	5.71	36.26	148
2	4	50	7.38	1.10	1.01	5.27	33.93	142
3	4	60	6.74	0.97	1.04	4.73	32.11	140
4	5	40	8.76	1.14	1.02	6.60	38.59	154
5	5	50	8.11	0.98	0.64	6.49	35.64	149
6	5	60	7.67	1.02	1.13	5.52	33.86	138
7	6	40	10.49	1.12	1.07	8.30	39.91	159
8	6	50	8.83	0.86	0.91	7.06	37.58	149
9	6	60	8.15	0.92	0.89	6.34	35.56	142

2.2. Optimization framework

In the current study, the multi-objective optimization problem, which balances the productivity and surface quality of the wall is defined as follows:

Find {*wfs* and *v*} to **maximize** {*EW* and *TH*} while **minimize** S_a.

Subject to the defined ranges of *wfs* and *v*.

To resolve this problem, an integrated optimization framework combining Entropy Weight Method (EWM) with COPRAS and WASPAS is proposed.

2.2.1. Entropy Weight Method (EWM)

The Entropy Weight Method (EWM) is an objective technique that determines response weights based on experimental data dispersion. By utilizing information entropy, this method eliminates subjective bias, ensuring that criteria with higher variability contribute more significantly to the decision-making process [18]. The procedure involves the following mathematical steps:

Step 1: Normalization of the decision matrix (r_{ij}). To eliminate the influence of different units, the decision matrix is normalized using the following relation [18]:

$$r_{ij} = \frac{x_{ij}}{\sum_{i=1}^{m} x_{ij}} \tag{2}$$

where x_{ij} represents the value of the i-th experimental run for the j-th response indicator, and m is the total number of experimental trials ($m = 9$).

Step 2: Calculation of the degree of entropy (e_j). The entropy value, which characterizes the uncertainty of information for each criterion, is calculated as [18]:

$$e_j = -\frac{1}{\ln m} \sum_{i=1}^{m} r_{ij} \cdot \ln r_{ij} \tag{3}$$

where $0 \le e_j \le 1$.

Step 3: Calculation of the diversification degree (d_j). The diversification degree represents the useful information provided by the j-th criterion. It is determined by the following formula [18]:

$$d_j = 1 - e_j \tag{4}$$

Step 4: Determination of the final objective weights (w_j). The final weight for each response indicator is calculated by normalizing the diversification degree [18]:

$$w_j = \frac{d_j}{\sum_{j=1}^{n} d_j} \tag{5}$$

where n is the total number of response indicators (*EW*, *TH*, and *Sa*).

The resulting weights derived from this process are subsequently utilized as the input for the COPRAS and WASPAS optimization methods to identify the optimal set of process parameters for the 20-layer Inconel 718 deposition.

2.2.2. COPRAS

The COPRAS method is utilized to evaluate alternatives by considering the direct and proportional influence of both maximizing (beneficial) and minimizing (cost) criteria on the

final results [19]. For the 20-layer Inconel 718 deposition process, the COPRAS procedure is implemented through the following steps:

Step 1: Normalization of the decision matrix (r_{ij}). To allow for the comparison of criteria with different units, the decision matrix is normalized using the following formula [19]:

$$r_{ij} = \frac{x_{ij}}{\sqrt{\sum_{i=1}^{m} x_{ij}}}, i = 1,...,m; j = 1,...,n \tag{6}$$

Step 2: Calculation of the weighted normalized decision matrix ($\hat{r}_{ij}$). The normalized values are adjusted by the objective weights (w_j) obtained from the EWM method [19]:

$$\hat{r}_{ij} = r_{ij} \cdot w_j \tag{7}$$

Step 3: Determination of maximizing S_i^+ and S_i^- minimizing indexes. The weighted normalized values are summed separately for beneficial criteria and cost criteria [19]:

$$S_i^+ = \sum_{j=1}^{g} \hat{r}_{ij} \quad \textit{(for Max criteria)} \tag{8}$$

$$S_i^- = \sum_{j=g+1}^{n} \hat{r}_{ij} \quad \textit{(for Min criteria)} \tag{9}$$

where g is the number of maximizing attributes.

Step 4: Calculation of the Relative Significance Value (R_i). The priority of each alternative is determined by its relative significance value [19]:

$$R_i = S_i^+ + \frac{\sum_{i=1}^{m} S_i^-}{S_i^- \cdot \sum_{i=1}^{m} \frac{1}{S_i^-}} \tag{10}$$

Step 5: Final Ranking. The alternatives are ranked in descending order of their R_i values. The alternative with the highest R_i (represented as R_{max}) is considered the optimal solution for the CMT-WAAM process.

2.2.3. WASPAS

The WASPAS method is a high-precision technique that enhances the reliability of the multi-objective optimization by integrating two separate models: the Weighted Sum Model (WSM) and the Weighted Product Model (WPM) [20]. For the 20-layer Inconel 718 CMT-WAAM deposition, the procedure is implemented through the following steps:

Step 1: Normalization of the decision matrix (r_{ij}). To transform criteria with different units into dimensionless values, the decision matrix is normalized based on the objective type:

For beneficial criteria (*EW*, *TH*) [20]:

$$r_{ij} = \frac{x_{ij}}{\max_i(x_{ij})} \tag{11}$$

For cost criteria (S_a) [20]:

$$r_{ij} = \frac{\min_i(x_{ij})}{x_{ij}} \tag{12}$$

Step 2: Determination of the Additive Relative Importance (WSM). The additive score ($Q_i^{(1)}$) for each experimental run is calculated by summing the products of the normalized values and their respective Entropy weights (w_j) [20]:

$$Q_i^{(1)} = \sum_{j=1}^{n} r_{ij} \cdot w_j \tag{13}$$

Step 3: Determination of the Multiplicative Relative Importance (WPM). The multiplicative score ($Q_i^{(2)}$) is obtained by calculating the product of the normalized values raised to the power of their weights [20]:

$$Q_i^{(2)} = \prod_{j=1}^{n} (r_{ij})^{w_j} \tag{14}$$

Step 4: Calculation of the Joint Generalized Criterion (Q_i). To achieve a robust ranking, the WSM and WPM scores are combined using a joint criterion. Following standard practice, a coefficient $\lambda = 0.5$ is applied to balance the additive and multiplicative importance [20]:

$$Q_i = \lambda \cdot Q_i^{(1)} + (1-\lambda) \cdot Q_i^{(2)} \tag{15}$$

Step 5: Final Ranking The alternatives are ranked in descending order based on their Q_i values. The parameter set with the highest score is identified as the optimal combination for maximizing the effective stacking width and height while minimizing surface irregularities.

3. RESULTS AND DISCUSSION

This section presents the relationships between the process parameters and the geometric characteristics of the 20-layer thin walls, followed by a multi-response optimization to determine the optimal process parameters.

3.1. Statistical analysis

In the current study, the analysis of variance (ANOVA) was conducted using Minitab at a 95% confidence level. A P-value inferior to 0.05 indicates statistical significance. The developed regression models of *EW*, *TH*, and S_a are described by Eq. (16), (17), and (18), respectively.

$$EW = -1.54 + 2.223\ wfs + 0.0555\ v - 0.0245\ wfs{\cdot}v \tag{16}$$

$$TH = 36.75 + 2.042\ wfs - 0.1955\ v - 0.0050\ wfs{\cdot}v \tag{17}$$

$$S_a = 108.1 + 14.56\ wfs + 0.436\ v - 0.2233\ wfs{\cdot}v \tag{18}$$

Table 4. ANOVA for *EW*.

Source	DF	Seq SS	Contribution	Adj SS	Adj MS	*F*-Value	*p*-Value
Regression	3	8.9135	97.56%	8.91352	2.97117	66.71	0.000
wfs	1	5.9800	65.45%	0.77037	0.77037	17.30	0.009
v	1	2.6934	29.48%	0.04800	0.04800	1.08	0.347
wfs·v	1	0.2401	2.63%	0.24010	0.24010	5.39	0.068
Error	5	0.2227	2.44%	0.22271	0.04454		
Total	8	9.1362	100.00%				
Model determination coefficients: R^2 = 97.56%, adjusted R^2 = 96.10%, predicted R^2 = 92.38%							

As shown in Table 4, the regression model of *EW* is highly significant, with an *F*-value of 66.71 and a *p*-value < 0.001, explaining 97.56% of the total variation in *EW*. The high adjusted R^2 (96.10%) and predicted R^2 (92.38%) further demonstrate the high accuracy and good prediction capability of the model. Among the investigated factors, *wfs* is the dominant parameter, contributing 65.45% of the total variation, followed by *v* with 29.48% of contribution. The interaction between *wfs* and *v* (*wfs*·*v*) contributes only 2.63%. The low error contribution (2.44%) indicates that the developed regression model adequately captures the relationship between the process parameters and *EW*, providing a reliable basis for subsequent process optimization.

Table 5. ANOVA for TH.

Source	**DF**	**Seq SS**	**Contribution**	**Adj SS**	**Adj MS**	***F*-Value**	***p*-Value**
Regression	3	48.4426	99.18%	48.4426	16.1475	200.55	0.000
wfs	1	19.2604	39.43%	0.6496	0.6496	8.07	0.036
v	1	29.1721	59.72%	0.5956	0.5956	7.40	0.042
wfs · *v*	1	0.0100	0.02%	0.0100	0.0100	0.12	0.739
Error	5	0.4026	0.82%	0.4026	0.0805		
Total	8	48.8452	100.00%				
Model determination coefficients: R^2 = 99.18%, adjusted R^2 = 98.68%, predicted R^2 = 98.02%							

Table 6 presents the ANOVA results for the surface roughness (S_a) model. The regression model is statistically significant, with an *F*-value of 49.88 and $p < 0.001$, explaining 96.77% of the total variation in S_a. Among the investigated parameters, travel speed (*v*) has the largest contribution (73.29%) but is statistically insignificant within the studied range ($p = 0.322$). In contrast, *wfs* has a contribution of 18.22% and significantly affects S_a ($p = 0.014$). The *wfs*·*v* interaction contributes 5.26% and is also statistically significant ($p = 0.036$), indicating that the combined effect of the two parameters should be considered when predicting surface roughness. The model exhibits good predictive performance, with R^2, adjusted R^2, and predicted R^2 values of 96.77%, 94.83%, and 89.86%, respectively. The relatively small difference between these coefficients and the low error contribution (3.23%) confirm that the regression model provides a satisfactory representation of the variation in Sa and can be used for subsequent multi-response optimization.

Table 6. ANOVA for S_a.

Source	**DF**	**Seq SS**	**Contribution**	**Adj SS**	**Adj MS**	**F-Value**	**P-Value**
Regression	3	367.01	96.77%	367.009	122.336	49.88	0.000
wfs	1	69.09	18.22%	33.019	33.019	13.46	0.014
v	1	277.98	73.29%	2.957	2.957	1.21	0.322
wfs · *v*	1	19.94	5.26%	19.936	19.936	8.13	0.036
Error	5	12.26	3.23%	12.262	2.452		
Total	8	379.27	100.00%				
Model determination coefficients: R^2 = 96.77%, adjusted R^2 = 94.83%, predicted R^2 = 89.86%							

Figure 3(a) shows the effects of *wfs* and *v* on the effective width (*EW*). *EW* increases markedly with increasing *wfs*, whereas it decreases with increasing *v*. This behavior is attributed to the greater volume of wire material supplied per unit time at higher *wfs*, resulting in a larger amount of deposited material and consequently a wider bead. In contrast, increasing *v* reduces the amount of material deposited per unit length, leading to a narrower wall. The contour plot confirms that the maximum *EW* is obtained at high wfs and low *v*, while the minimum *EW* occurs under the opposite conditions. The relatively steep slope of the main-effects curve for *wfs* also indicates that *EW* is particularly sensitive to changes in wire feed speed, consistent with the ANOVA results, which identified wfs as the most significant factor for *EW*.

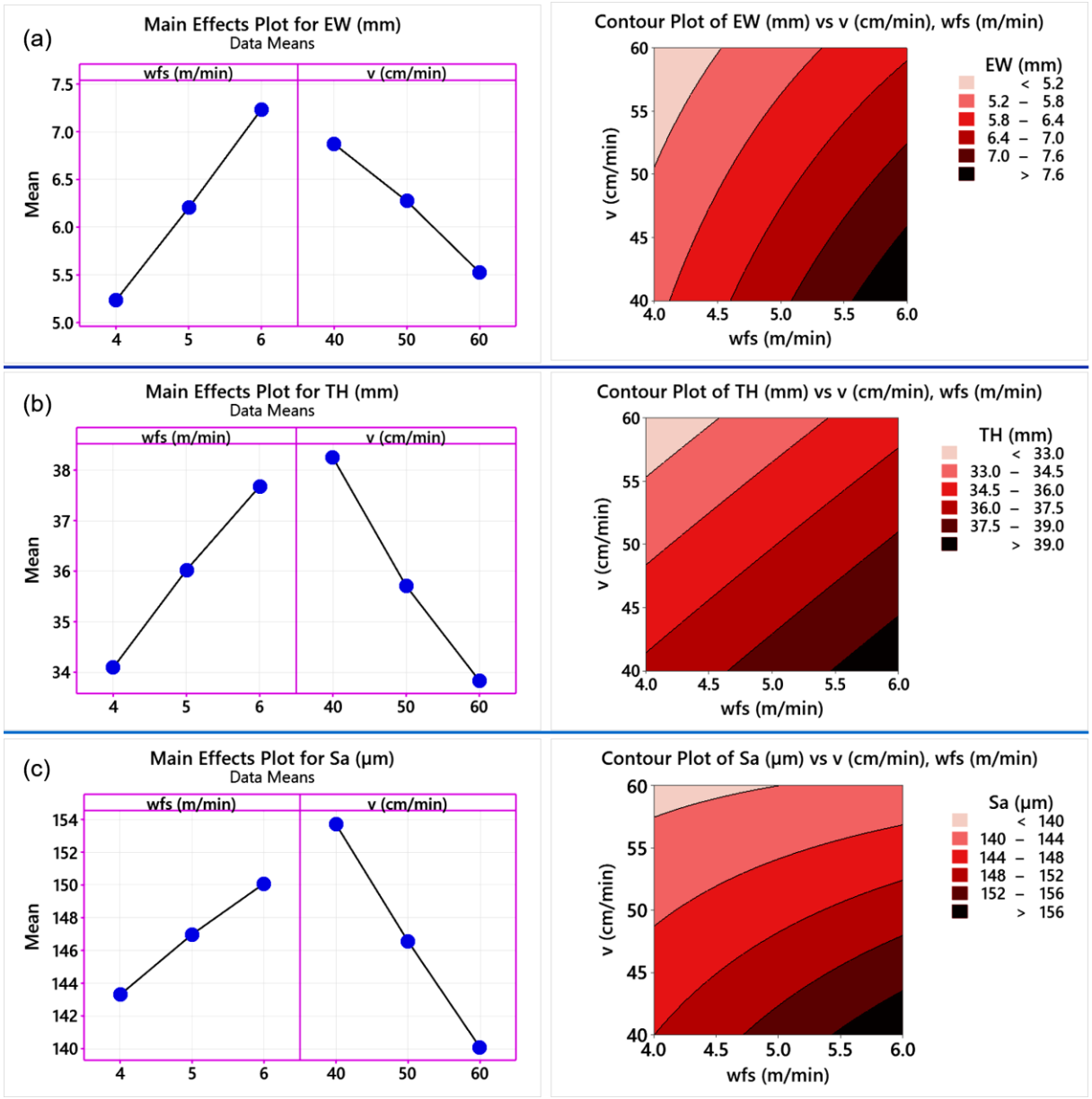


Figure 3. Main effects (on the left) and interaction effects (on the right) of *wfs* and *v* on (a) *EW*, (b) *TH*, and (a) S_a.

The variation in total height (*TH*) with the process parameters is presented in Fig. 3(b). *TH* increases with increasing *wfs* but decreases substantially with increasing *v*. The increase in *TH* at higher *wfs* results from the higher material deposition rate, which promotes greater accumulation of material over the 20 deposited layers. Conversely, a higher travel speed reduces the deposited material per unit length and consequently decreases the accumulated wall height. Compared with *wfs*, *v* exhibits a more pronounced effect on *TH*, as indicated by the steeper main-effects trend and its larger contribution in the ANOVA analysis. The contour plot further demonstrates that the highest *TH* is achieved at high *wfs* combined with low *v*. These results highlight the importance of controlling travel speed when targeting a specific wall height.

Figure 3(c) illustrates the effects of wfs and v on the surface roughness (S_a). In general, S_a increases with increasing *wfs* and decreases with increasing *v*. Higher *wfs* increases the material deposition rate, which can promote greater bead accumulation and surface irregularities, thereby increasing surface roughness. Conversely, increasing *v* reduces the deposited material per unit length and tends to produce a more uniform surface profile. The contour plot reveals a nonlinear response, particularly at higher wfs, indicating that the effect of one parameter depends partly on the level of the other. This observation agrees with the ANOVA results, where the *wfs*·*v* interaction was found to be statistically significant. Overall, relatively low wfs and high v are favorable for minimizing S_a, although these conditions must be balanced against the requirements for achieving adequate wall width and height.

3.2. Multi-objective optimization results

To address the trade-off between deposition efficiency and surface quality, a multi-criteria decision-making (MCDM) framework was employed. The Entropy Weight Method (EWM) was first utilized to objectively determine the relative importance of each response based on the inherent dispersion of the experimental data, thereby eliminating subjective bias. The calculated entropy values (e_j), diversification degrees (d_j), and final weights (w_j) for the three criteria are summarized in Table 5.

Table 5. Computing the entropy weights for the responses.

Criterion	Entropy (e_j)	Diversification (d_j)	Weight (w_j)
EW	0.9941	0.0059	0.807
TH	0.9990	0.0010	0.132
Sa	0.9996	0.0004	0.061
Total			1.000

The results indicate that the effective width (*EW*) received the highest weight (0.807), followed by the total height (*TH*) (0.132) and surface roughness (S_a) (0.061). This confirms that deposition efficiency is the dominant criteria in evaluating the 20-layer CMT-WAAM process. These weights were subsequently integrated into the COPRAS and WASPAS methods to identify the optimal processing conditions.

The multi-objective optimization results obtained using the COPRAS and WASPAS methods are summarized in Table 6. For WASPAS, $Q^{(1)}$ and $Q^{(2)}$ represent the additive (WSM) and multiplicative (WPM) scores, respectively, while Q is the combined generalized criterion ($\lambda = 0.5$). For COPRAS, S_i^+ and S_i^- are the weighted sums for beneficial criteria (*EW*, *TH*) and cost criterion (S_a), respectively, and R_i is the relative significance value.

Table 6. Summary of ranking results for different MCDM methods.

Run	Parameters		WASPAS				COPRAS			
	wfs **(m/min)**	***v*** **(cm/min)**	$Q_i^{(1)}$	$Q_i^{(2)}$	Q_i	**Rank**	S_i^+	S_i^-	R_i	**Rank**
1	4	40	0.7187	0.7106	0.7147	6	0.0963	0.0076	0.1039	6
2	4	50	0.6682	0.6584	0.6633	8	0.0891	0.0074	0.0968	8
3	4	60	0.6078	0.5928	0.6003	9	0.0807	0.0072	0.0886	9
4	5	40	0.8253	0.8213	0.8233	3	0.1100	0.0079	0.1171	3
5	5	50	0.8078	0.8050	0.8064	4	0.1071	0.0077	0.1145	4
6	5	60	0.7001	0.6916	0.6959	7	0.0926	0.0071	0.1007	7
7	**6**	**40**	**0.9903**	**0.9896**	**0.9900**	**1**	**0.1346**	**0.0082**	**0.1416**	**1**
8	6	50	0.8711	0.8700	0.8706	2	0.1161	0.0076	0.1237	2
9	6	60	0.7958	0.7925	0.7942	5	0.1050	0.0075	0.1127	5

The results show strong agreement between the two methods, with all nine experimental runs achieving identical rankings across both COPRAS and WASPAS. This high level of consistency demonstrates the robustness of the proposed optimization framework. Run 7 (*wfs* = 6 m/min, *v* = 40 cm/min) is consistently identified as the best-performing condition, achieving the highest performance values in both WASPAS (Q = 0.9900) and COPRAS (R = 0.1416). In contrast, Run 3 (*wfs* = 4 m/min, *v* = 60 cm/min) is ranked as the least favorable condition by both methods.

The selection of Run 7 as the optimal condition can be explained by the balance between deposition efficiency and surface stability. A high wire feed speed (6 m/min) ensures sufficient material input, resulting in a substantial wall height. These results align with previous findings in CMT-based WAAM of Inconel 718. Shi et al. [21] reported that moderate travel speeds (40 - 60 cm/min) combined with high wire feed speeds (5 - 7 m/min) yield optimal geometric stability. Similarly, Dinh et al. [17] observed that excessive heat input at low travel speeds (≤ 40 cm/min) leads to increased surface roughness, while high travel speeds (≥ 60 cm/min) reduce deposition height. The present results confirm these observations, further validating the identified optimal parameter window.

4. CONCLUSION

This study systematically optimized the process parameters for the deposition of 20-layer Inconel 718 thin walls by CMT-WAAM. The main conclusions are summarized as follows:

- The geometric characteristics and surface quality are strongly governed by the interaction between wire feed speed (*wfs*) and travel speed (*v*). Wire feed speed primarily controls the effective width (*EW*), contributing to 65.45% of the total variance, while travel speed has the most significant influence on total height (*TH*) and surface roughness (S_a), contributing 59.72% and 69.67%, respectively.

- The developed regression models exhibit high accuracy, with coefficients of determination (R^2) of 97.56% for *EW*, 99.18% for *TH*, and 96.77% for S_a, confirming their reliability in predicting multilayer deposition behavior within the investigated parameter range.

- The combined COPRAS and WASPAS optimization results consistently identified Run 7 (*wfs* = 6 m/min, *v* = 40 cm/min) as the optimal condition, achieving the highest performance scores in both methods. The optimized process parameters provide a favorable balance between deposition geometry and surface quality for the investigated 20-layer Inconel 718 thin walls.

- The strong agreement between the two MCDM methods, with all nine experimental runs achieving identical rankings, confirms the robustness and consistency of the proposed optimization framework. The integration of Entropy Weight Method with COPRAS and WASPAS demonstrates its effectiveness as a decision support tool for multi-response optimization in CMT-based additive manufacturing of nickel-based superalloys.

Further investigations are recommended to extend the parameter range, explore advanced CMT variants, and evaluate the microstructure and mechanical properties of the fabricated thin walls. Additionally, incorporating in-process thermal monitoring and closed-loop control could further enhance geometric stability in taller multilayer structures.

ACKNOWLEDGMENT

This research is funded by Vietnam National Foundation for Science and Technology Development (NAFOSTED) under grant number 107.99-2023.17.

REFERENCES

[1]. F. He, L. Yuan, J. Yang, W. Zhou, Y. Zhang, Z. Pan, H. Li, Process innovations in wire arc additive manufacturing systems: progress, challenges and future opportunities, Progress in Materials Science. 163 (2027) 101776. https://doi.org/10.1016/j.pmatsci.2026.101776

[2]. B. Das, N. Sahoo, P. Patel, A. Ghosh, M.A. Khan, B. Bhushan, R. Madan, P. Shrivastava, V. Msomi, Wire Arc Additive Manufacturing (WAAM): A comprehensive review of process, materials, modelling, artificial intelligence, and industrial applications, Journal of Alloys and Compounds. 1058 (2026) 186347. https://doi.org/10.1016/j.jallcom.2026.186347

[3]. F. Lambiase, P.B. Yanala, F. Pace, E. Andreucci, A. Paoletti, A state of the art review of wire arc additive manufacturing (WAAM)-part 1: process fundamentals, parameters and materials, The International Journal of Advanced Manufacturing Technology. 138 (2025) 4965-4993. https://doi.org/10.1007/s00170-025-15781-8

[4]. V.T. Le, D.M. Dinh, V.-C. Tran, Q.H. Mai, Q.H. Pham, Machine learning-based prediction models of single weld bead attributes in wire arc additive manufacturing of Inconel 625 superalloy and process map generation, International Journal of Pressure Vessels and Piping. 219 (2026) 105659. https://doi.org/10.1016/j.ijpvp.2025.105659

[5]. Q. Shen, J. Xue, Z. Zheng, X. Yu, N. Ou, Machine learning-based prediction of CoCrFeNiMo0.2 high-entropy alloy weld bead dimensions in wire arc additive manufacturing, Materials Today Communications. 41 (2024) 110359. https://doi.org/10.1016/j.mtcomm.2024.110359

[6]. R. Mamedipaka, M. Hemachandra, A. Mishra, S. Sinhmar, S. Thapliyal, Machine learning-assisted wire arc additive manufacturing and heat input effect on mechanical and corrosion behaviour of 316 L stainless steels, Structures. 68 (2024) 107126. https://doi.org/10.1016/j.istruc.2024.107126

[7]. P. Saravanamuthukumar, A.B. Abdullah, Z.K. Wani, Machine learning-based prediction and optimization of WAAM process parameters for enhanced deposition efficiency, Progress in Additive Manufacturing. 10 (2025) 11093-11107. https://doi.org/10.1007/s40964-025-01276-1

[8]. V.T. Le, D.M. Dinh, V.-C. Tran, M. Muzamil, Modelling, analysis, and multi-objective optimization of single weld bead characteristics in wire arc additive manufacturing of Inconel 625 based on machine learning and NSGA-II, Materials Today Communications. 49 (2025) 113831. https://doi.org/10.1016/j.mtcomm.2025.113831

[9]. H. Mirabi, F. Mirakhorli, J.F. Béland, F. Nadeau, V. Demers, P. Bocher, On selecting proper process parameters for cold metal transfer (CMT)-based wire arc additive manufacturing (WAAM) process, International Journal of Advanced Manufacturing Technology. 133 (2024) 6083-6093. https://doi.org/10.1007/s00170-024-14110-9

[10]. D.M. Dinh, V.T. Le, Wire and arc additive manufacturing of Inconel alloys: A review on microstructures, mechanical properties, and common defects, Journal of Science and Technology - HaUI. 60 (2024) 20-23. https://doi.org/10.57001/huih5804.2024.176

[11]. M. Chandra, K.E.K. Vimal, S. Rajak, A comparative study of machine learning algorithms in the prediction of bead geometry in wire-arc additive manufacturing, International Journal on Interactive Design and Manufacturing (IJIDeM). 18 (2024) 6625-6638. https://doi.org/10.1007/s12008-023-01326-4

[12]. D. Ding, F. He, L. Yuan, Z. Pan, L. Wang, M. Ros, The first step towards intelligent wire arc additive manufacturing: An automatic bead modelling system using machine learning through industrial information integration, Journal of Industrial Information Integration. 23 (2021) 100218. https://doi.org/10.1016/j.jii.2021.100218

[13]. Z. Zhang, J. Yan, X. Lu, T. Zhang, H. Wang, Optimization of porosity and surface roughness of CMT-P wire arc additive manufacturing of AA2024 using response surface methodology and NSGA-II, Journal of Materials Research and Technology. 24 (2023) 6923-6941. https://doi.org/10.1016/j.jmrt.2023.04.259

[14]. R.M. Kindermann, M.J. Roy, R. Morana, P.B. Prangnell, Process response of Inconel 718 to wire + arc additive manufacturing with cold metal transfer, Materials and Design. 195 (2020) 109031. https://doi.org/10.1016/j.matdes.2020.109031

[15]. R.M. Kindermann, M.J. Roy, R. Morana, J.A. Francis, Effects of microstructural heterogeneity and structural defects on the mechanical behaviour of wire + arc additively manufactured Inconel 718 components, Materials Science and Engineering A. 839 (2022) 142826. https://doi.org/10.1016/j.msea.2022.142826

[16]. F.R. Teixeira, F.M. Scotti, L.O. Vilarinho, C.A.M. da Mota, A. Scotti, Transferability of the working envelope approach for parameter selection and optimization in thin wall WAAM, International Journal of Advanced Manufacturing Technology. 119 (2022) 969-989. https://doi.org/10.1007/s00170-021-08326-2

[17]. D.M. Dinh, H.S. Lam, V.T. Le, Q.H. Pham, Evaluation of the forming quality of Inconel 625 thin-walled parts manufactured via cold metal transfer additive manufacturing, Science & Technology Development Journal. 27 (2024) 3570-3582. https://doi.org/10.32508/stdj.v27i3.4308

[18]. V.T. Le, L. Hoang, M.F. Ghazali, V.T. Le, M.T. Do, T.T. Nguyen, T.S. Vu, Optimization and comparison of machining characteristics of SKD61 steel in powder-mixed EDM process by TOPSIS and desirability approach, The International Journal of Advanced Manufacturing Technology. 130 (2024) 403-424. https://doi.org/10.1007/s00170-023-12680-8

[19]. S.H. Mousavi-Nasab, A. Sotoudeh-Anvari, A comprehensive MCDM-based approach using TOPSIS, COPRAS and DEA as an auxiliary tool for material selection problems, Materials & Design. 121 (2017) 237-253. https://doi.org/10.1016/j.matdes.2017.02.041

[20]. A. Radomska-Zalas, Application of the WASPAS method in a selected technological process, Procedia Computer Science. 225 (2023) 177-187. https://doi.org/10.1016/j.procs.2023.10.002

[21]. J. Shi, N. Qian, S. Sun, Y. Kaynak, R. Das, Y. Fu, H. Su, Effect of process parameters on microstructure and properties of Inconel-718 superalloy fabricated by wire-arc direct energy deposition technique, Journal of Materials Research and Technology. 37 (2025) 173-185. https://doi.org/10.1016/j.jmrt.2025.06.026